Processing and Fabrication of Advanced Materials - XIX

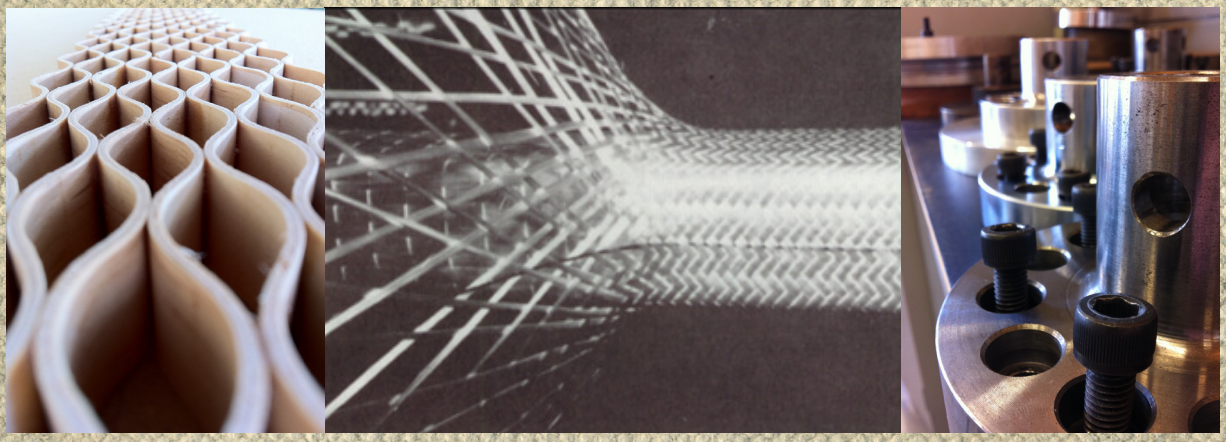

Auckland, New Zealand, January 2011

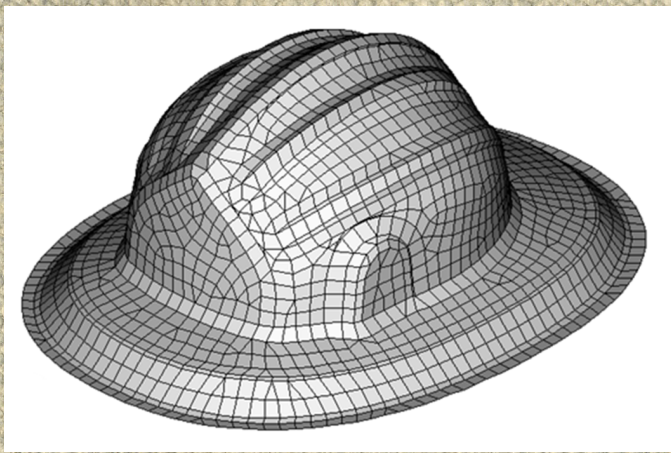

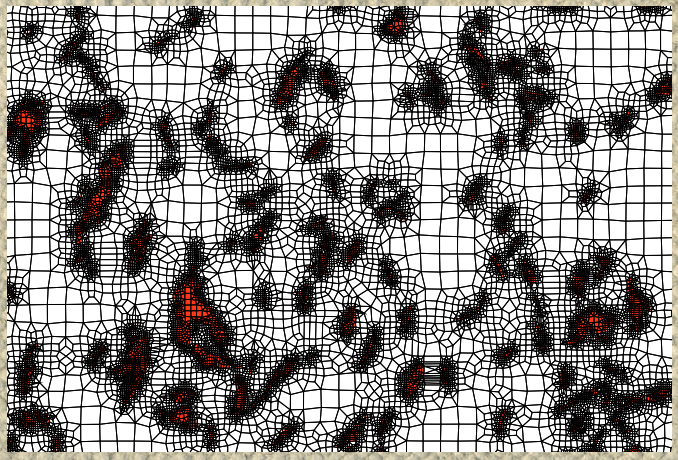

Editors:
D. Bhattacharyya
R.J.T. Lin
T.S. Srivatsan

Processing and Fabrication of Advanced Materials XIX

Editors:
D. Bhattacharyya
R.J.T. Lin
T.S. Srivatsan

Processing and Fabrication of Advanced Materials XIX

Proceedings of an International Conference organized by:

The Centre for Advanced Composite Materials
The University of Auckland
New Zealand

January 14-17, 2011

The University of Auckland
Auckland, New Zealand

Hard copy: ISBN 978-0-473-18178-9 (set)
Electronic copy: ISBN 978-0-473-18189-5

Preface

These volumes contain the papers presented at the ***Nineteenth International Conference on Processing and Fabrication of Advanced Materials (PFAM XIX)*** held in Auckland, New Zealand, during **January 14-17, 2011**. The ***Centre for Advanced Composite Materials housed within the Faculty of Engineering***, at **the University of Auckland** (Auckland, New Zealand), was the principal organiser that put together this international conference spread over four days. It is the NINETEENTH in a series of conferences bringing together engineers, technologists, and researchers from industry, universities and research laboratories, working on various aspects related to the processing, fabrication, characterisation and evaluation of both advanced and emerging materials. The idea is to share and discuss their research findings, observations and inferences. The earlier conferences were held as follows:

(1) The ***first*** was held in Cincinnati (USA) in **1991**
(2) The ***second*** was held in Chicago (USA) in **1992**
(3) The ***third*** was held in Pittsburgh (USA) in **1993**
(4) The ***fourth*** in Cleveland (USA) in **1995**
(5) The ***fifth*** in Cincinnati (USA) in **1996**
(6) The ***sixth*** in Singapore (Singapore) in **1997**
(7) The ***seventh*** was held in Rosemont, Illinois (USA) in **1998**
(8) The ***eighth*** was held in Singapore (Singapore) in **1999**
(9) The ***ninth*** was held in St. Louis, Missouri (USA) in **2000**
(10) The ***tenth*** was held in Indianapolis, Indiana (USA) in **2001**
(11) The ***eleventh*** was held in Columbus, Ohio (USA) in **2002**
(12) The ***twelfth*** was held at Pittsburgh, PA (USA) in **2003**
(13) The ***thirteenth*** was held in Singapore (Singapore) in **2004**
(14) The ***fourteenth*** was held in Pittsburgh, PA (USA) in **2005**
(15) The ***fifteenth*** was held in Cincinnati, OH (USA) in **2006**
(16) The ***sixteenth*** was held in Singapore (Singapore) in **2007**
(17) The ***seventeenth*** was held in New Delhi (India) in **2008.**
(18) The ***eighteenth*** was held in Sendai (Japan) in **2009.**

This conference is a collection of papers from over 30 countries. Over 200 abstracts that include both invited and contributed papers, were received and reviewed for oral/poster presentations. More than 100 manuscripts that were received in time were reviewed again for inclusion in both the bound and electronic volumes, the latter allowing us to include a few late submissions. The papers cover a spectrum of topics that represent a truly diverse nature of the field of materials science and engineering and related manufacturing processes. On behalf of the Organising Committee, we extend our warmest thanks and appreciation to the authors of the manuscripts, session chairs and sponsors for their interest, enthusiasm and support. Sincere thanks are also due to the technical editors, co-organisers and the members of the advisory committees, both local and international.

International Organisers

Prof. Debes Bhattacharyya
Centre for Advanced Composite Materials
Department of Mechanical Engineering
The University of Auckland
Auckland
New Zealand

Dr. Alan Kin Tak Lau
Centre of Excellence in Engineered Fibre Composites
Department of Mechanical Engineering
University of Southern Queensland
Toowoomba
Australia

Dr. Richard J.T. Lin
Centre for Advanced Composite Materials
Department of Mechanical Engineering
The University of Auckland
Auckland
New Zealand

Prof. Naresh Bhatnagar
Department of Mechanical Engineering
Indian Institute of Technology (IIT) Delhi
Hauz Khas, New Delhi 110 016
India

Prof. Tirumalai. S. Srivatsan
Division of Materials Science and Engineering
Department of Mechanical Engineering
The University of Akron
Akron, Ohio 44325-3903
USA

Organising Committee

Member	Affiliation	Country
Prof. Debes Bhattacharyya (Chair)	**University of Auckland**	**New Zealand**
Prof. Tirumalai S. Srivatsan	**University of Akron**	**USA**
Prof. Naresh Bhatnaghar	**Indian Institute of Technology, IIT (Delhi)**	**India**
Dr. Alan Kin-tak Lau	**Uni. of Southern Queensland**	**Australia**
Dr. Richard J.T. Lin (Secretary)	**University of Auckland**	**New Zealand**
Prof. Stoyko Fakirov	**University of Auckland**	**New Zealand**
Assoc. Prof. Simon Bickerton	**University of Auckland**	**New Zealand**
Assoc. Prof. Allan Easteal	**University of Auckland**	**New Zealand**
Dr. Sourish Banerjee	**University of South Queensland**	**Australia**
Dr. Mark Battley	**University of Auckland**	**New Zealand**
Dr. Raj Das	**University of Auckland**	**New Zealand**
Dr. Yu Dong	**University of Auckland**	**New Zealand**
Dr. Miro Duhovic	**IVW, University of Kaiserslautern**	**Germany**
Dr. Krishnan Jayaraman	**University of Auckland**	**New Zealand**
Dr. Jim Lee	**University of Auckland**	**New Zealand**
Dr. Dongyan Liu	**University of Auckland**	**New Zealand**
Dr. Xiaowen Yuan	**University of Auckland**	**New Zealand**
Dr. Sanjeev Rao	**University of Auckland**	**New Zealand**
Dr. Anjaneya Prasad Penneru	**University of Auckland**	**New Zealand**
Ms. Syamali Bhattacharyya	**Uniservices Ltd**	**New Zealand**
Ms. Sheeja Chidambaram	**University of Auckland**	**New Zealand**

International Advisory Committee

Member	Affiliation	Country
Prof. Suresh G Advani	**University of Delaware**	**USA**
Prof. Mathias Brieu	**Ecole centrale, Lille**	**France**
Prof. Klaus Friedrich	**Institut fuer Verbundwerkstoffe GmbH**	**Germany**
Prof. Anup Ghosh	**Indian Institute of Technology (IIT Delhi)**	**India**
Prof. Patricia Krawzak	**Ecole de Mine, Douai**	**France**
Prof. Anil Netravali	**Cornell University**	**USA**
Prof. Y.K.D.V.Prasad	**University of Queensland**	**Australia**
Dr. Dinesh Agarwal	**Pennsylvania State University**	**USA**
Dr. Manoj Gupta	**National University of Singapore**	**Singapore**
Dr. Satish Kailas	**Indian Institute of Science**	**India**
Dr. K.U. Kainer	**GKSS Research Center**	**Germany**
Dr. Kamal Kar	**Indian Institute of Technology (IIT Kanpur)**	**India**
Dr. Masaaki Nakai	**Tohoku University**	**Japan**
Dr. Mitsuo Niimoni	**Tohoku University**	**Japan**
Dr. John Yong Ming Shyan	**SIMTech**	**Singapore**
Dr. Raghavan Srinivasan	**Wright State University**	**USA**
Dr. S.K. Thakur	**Delphi Automotive Systems**	**Singapore**
Prof. Jens Schuster	**University of Applied Sciences Kaiserslautern**	**Germany**
Dr. Sébastien Comas-Cardona	**Ecole des Mines de Douai**	**France**

Local Advisory Committee

Member	Affiliation
Prof. John Chen	**University of Auckland**
Prof. Roy Crawford	**University of Waikato**
Prof. George Ferguson	**University of Auckland**
Prof. Wei Gao	**University of Auckland**
Dr. Mark Jones	**University of Auckland**
Dr. Michelle Dickinson	**University of Auckland**
Dr. Alan Fernyhough	**Scion**
Dr. Zhan Chen	**Auckland University of Technology**
Prof. Deliang Zhang	**University of Waikato**
Dr. Kim Pickering	**University of Waikato**
Dr. Mark P Staiger	**University of Canterbury**

Technical Editors

Member	Affiliation
Peter Lescher	**University of Auckland**
Ryan McCardle	**University of Auckland**
Peng Shaun Tan	**University of Auckland**

Plenary and Keynote Speakers

Member	Affiliation	Country
Prof. Roy Crawford	**University of Waikato**	**New Zealand**
Prof. Klaus Friedrich	**Institut fuer Verbundwerkstoffe GmbH**	**Germany**
Dr. Andrew Beehag	**CRC for Advanced Composite Structures**	**Australia**
Prof. Naresh Bhatnagar	**Indian Institute of Technology (IIT Delhi)**	**India**
Prof. Anil K Bhowmick	**Indian Institute of Technology (IIT Patna)**	**India**
Prof. Christoph Binetruy	**Ecole des Mines de Douai**	**France**
Prof. Ralph Cooney	**University of Auckland**	**New Zealand**
Prof. Alan Crosky	**University of New South Wales**	**Australia**
Prof. Pascal Hubert	**McGill University**	**Canada**
Prof. Eugene Joseph	**Virginia Tech**	**USA**
Prof. Karl U. Kainer	**GKSS Research Center**	**Germany**
Prof. Byung Sun Kim	**Korea Institute of Materials Science**	**Republic of Korea**
Prof. Alan Kin-Tak Lau	**University of Southern Queensland**	**Australia**
Prof. Woo Il Lee	**Seoul National University**	**Republic of Korea**
Prof. Peter Mitschang	**Institut für Verbundwerkstoffe GmbH**	**Germany**
Prof. Mitsuo Niinomi	**Tohoku University**	**Japan**
Prof. Robert Shanks	**RMIT University**	**Australia**
Prof. Tirumalai Srivatsan	**The University of Akron**	**USA**
Prof. Manfred Stamm	**Leibniz Institute of Polymer Research**	**Germany**
Prof. Norbert Stribeck	**University of Hamburg**	**Germany**
Prof. Ramesh Talreja	**Texas A&M University**	**USA**
Prof. Vikram Yadama	**Washington State University**	**USA**

Contents

Nanodeformation of Polymers and Polymer-based Nanocomposites Assessed by in-situ SAXS Measurements

Ahmad Zeinolebadi
TMC Institute, Hamburg University, Bundesstrasse 45, 20146 Hamburg, Germany
Norbert Stribeck
TMC Institute, Hamburg University, Bundesstrasse 45, 20146 Hamburg, Germany
Morteza Ganjaee Sari
TMC Institute, Hamburg University, Bundesstrasse 45, 20146 Hamburg, Germany

Abstract

Understanding the structure-property relationship of polymers and polymer based (nano)composites is a key to design materials with desired properties. X-ray scattering is an effective method to investigate structural variations of polymers from molecular scale to micron-size domains. A variety of polymers including thermoplastics, thermoplastic polyurethane elastomers and polymer composites and nanocomposites have been subjected to uniaxial mechanical deformation, while the evolution of the nano-structure has been monitored by two-dimensional small angle X-ray scattering. Data evaluation methods and theories are discussed briefly. Aided by the image processing language PV-*WAVE*, hundreds of SAXS patterns are processed automatically to yield nano-structure parameters describing size and arrangements of crystallites and other kinds of domains. Nano-structure parameters are evaluated by the chord distribution function (CDF) method. For example, the nanoscopic strain is determined and compared to macroscopic strain. Finally, some mechanisms are proposed to describe structural evolutions of polymeric materials at the nano scale.

Introduction

Understanding structure-property relationship is vital to fabricating polymeric materials with tailored mechanical properties. Hence, it is important to follow transient microstructures while loading the material. To achieve this goal it is essential to apply characterization methods by which the variations of

microstructure can be monitored during mechanical testing without disturbing it or affecting the mechanical properties. In other words, the characterization method must not cause any microstructural variations by itself and it must be executable without stopping the loading.

X-rays do not interact with polymers, thus they fulfill the above mentioned requirements. Therefore, time-resolved x-ray scattering experiments have been applied as effective direct methods to follow microstructural variations of polymeric materials under thermal and mechanical loads [1-3]. One challenge of this kind of experiments is, however, the huge number of grabbed patterns. Hence, fast automated computer programs are required to accelerate data evaluation and to reduce the ultimate analysis time.

We apply small-angle x-ray scattering to monitor the transient structure of different classes of polymeric materials such as polymer based (nano)composites, thermoplastics, elastomers and polymer blends. In this paper, the experimental methods and the basic theories are discussed briefly and some recent data are presented.

Experimental

Materials

Four types of materials have been used:

Types I and II: Isotactic polypropylene Moplen HP400R (density 0.905 g/cm^3, melt flow rate 25 g/10 min (230 °C, 2.16 kg), tensile modulus 1.35 GPa) has been purchased from Basell Polyolefins (Basell, Switzerland). Polypropylene is mixed with multi-wall carbon nanotubes using an extruder and cut into granules (mixing process has been done by JC Christiansen et al., at Aalborg University, Denmark). The granules are then injected molded at 200 °C into a standard test bar (dog-bone, gauge area 2 mm × 1 mm) using a laboratory hot press. The pure PP and the nanocomposite samples are labeled as Moplen and Mopnan, respectively.

Type III: A microfibrillar reinforced composite is made from 80 wt.-% high-density polyethylene (HDPE) and 20 wt.-% polyamide 6 (PA6). Details concerning the principle of the preparation [4], the design of the extruder line, and the making of the studied material have been published elsewhere [1].

Type IX: Commercial grade polyurethane (soft segments: linear polycaprolactone diol, chain extender: HQEE and Hard segments: MDI) with shore A of 95 is used. The samples are injected molded at 205, 215 and 235 °C and labeled as TPU205,

TPU215 and TPU235, respectively.

Mechanical tests

Mechanical tests in the X-ray beam are performed by a self-made tensile machine. The machine performs symmetric drawing. Signals from load cell and transducer are recorded during the experiment. In tensile tests the sample is stretched continuously and in load cycling after approaching a pre-strain the samples are cycled between two fixed distances of the cross-heads. Thus, strain-controlled load-cycling instead of stress controlled cycling is performed. During the tests a video camera monitors the sample and captures 2 pictures per cycle of the X-ray detector. Determination of the local macroscopic strain ε , is based on the recorded video frames. The method has recently been published [1].

In-situe SAXS measurements

SAXS is performed at the synchrotron beamline A2 at HASYLAB, Hamburg, Germany. The wavelength of the X-ray beam is 0.15 nm. Scattering patterns are collected by a 2D detector (marccd 165; mar research, Norderstedt, Germany) operated in 1024 × 1024 pixel mode (pixel size: 158.2 × 158.2 μm^2). Thus, for the typical long period of 20 nm a variation of the peak position by one pixel causes a long-period variation of below 1%.

Data evaluation

The basic data evaluation steps are documented in a text book [5]. The scattering patterns $I(s_{12}, s_3)$, $s=(s^2_{12} + s^2_3)^{0.5}$, are normalized to the flux of the incident primary beam. Intensity loss due to absorption in the sample is compensated using the measured intensities of the primary beam before and after the sample, respectively. The machine background is subtracted, after which the pixels in the shade of the beam stop and outside the bordering vacuum tube are marked invalid. The fiber pattern is centered and aligned. Part of the invalid regions can be filled from symmetry consideration. The remnant central blind hole is filled applying a stiff parabolic extrapolation [6]. The pattern is projected on the representative fiber plane. Multiplication by s^2 applies the real-space Laplacian. The density fluctuation background is determined by low-pass filtering. It is eliminated by subtraction. The resulting interference function, $G(s_{12}, s_3)$ describes the ideal multiphase system. Its 2D Fourier transform is the chord distribution function (CDF), $z(r_{12}, r_3)$. From $G(s_{12}, s_3)$ the scattering intensity $I_{id}(s_{12}, s_3)$ of the ideal multiphase system can be reconstructed. From this pattern the scattering power

$$Q = \iiint I_{id}(s)\, d^3 s \qquad (1)$$

is computed. Q is already normalized with respect the to the irradiated volume, because of the respective normalization of the measured intensity. For this normalization we have taken advantage of the fact that the cross-section of the primary beam is oblong with its long axis (3 mm) perpendicular to the fiber. Thus, the taut fiber sample is totally immersed in the primary beam. Now assuming incompressibility, a quantity that is proportional to the irradiated volume can be estimated from the initial diameter of the fiber and the actual macroscopic strain ε(t), where t is the time elapsed during the experiment. Because the major fraction of the studied materials is made from semicrystalline polyethylene, a major contribution [1,5,7] to the invariant

$$Q = v(1 - v)(\rho_c - \rho_a)^2 + X \qquad (2)$$

originates from the two-phase structure of the polyethylene with v being its volume crystallinity, and ρ_c - ρ_a the contrast between the crystalline and the amorphous electron density. The unknown quantity X is predominantly originating from the embedded reinforcing needle-shaped domains (PA6), and from voids. In addition, the nanoscopic strain ε_{nano}, is estimated from the variation of the long period peaks in CDF.

Results and discussion

In the following sections the results regarding four different types of materials will be presented.

PP and PP/MWCNT nanocomposite: SAXS patterns and the corresponding CDFs of Moplen and Mopnan samples at different stages of load cycling are presented in Figs. 1 and 2, respectively. The strong meridional drop-shaped peaks indicate that both samples are highly oriented in their initial state [8,9]. As the sample is deformed the meridional peaks become weaker in intensity and move closer to the center. In both cases the meridional peak consist of a strong drop-shaped peak imposed on a broader and weaker elliptical peak. The drop-shaped peak is attributed to an oriented lamellar-stack structure with its axis parallel to the axis of the tensile bar. The weak elliptical peak observed in the original material can be explained by an ensemble of lamellar stacks with random orientation, in which the long period is a function of the stack's inclination with respect to the axis of the

injection-molded tensile bar. Notably, the long period in transverse direction is longer than that in longitudinal direction.

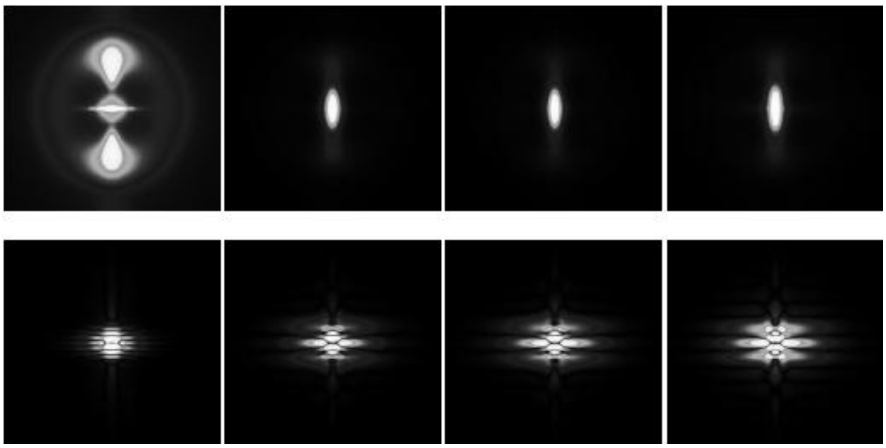

Figure 1: SAXS patterns (1st row) and CDF (2nd row) of Moplen sample at different stages of load cycling: a) ε = 0, b) first maximum ε, c) first minimum ε and d) end of cycling

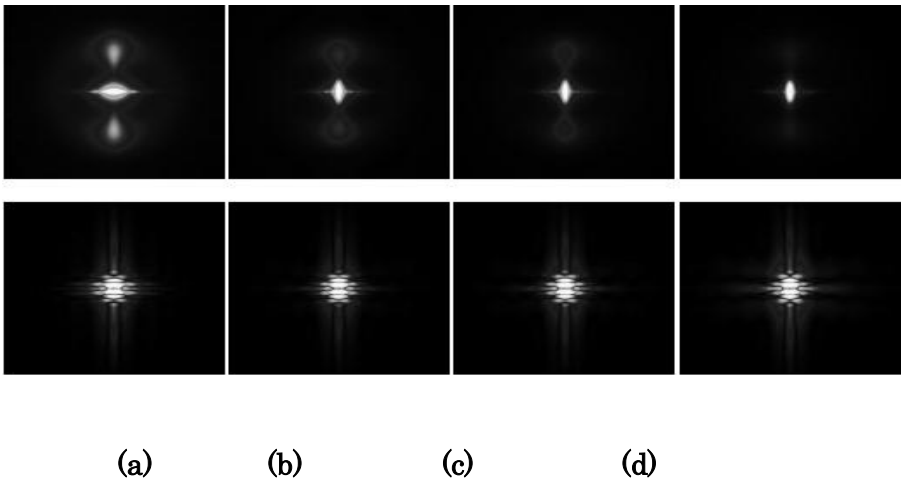

Figure 2: SAXS patterns (1st row) and CDF (2nd row) of Mopnan sample at different stages of load cycling: a) ε = 0, b) first maximum ε, c) first minimum ε and d) end of cycling

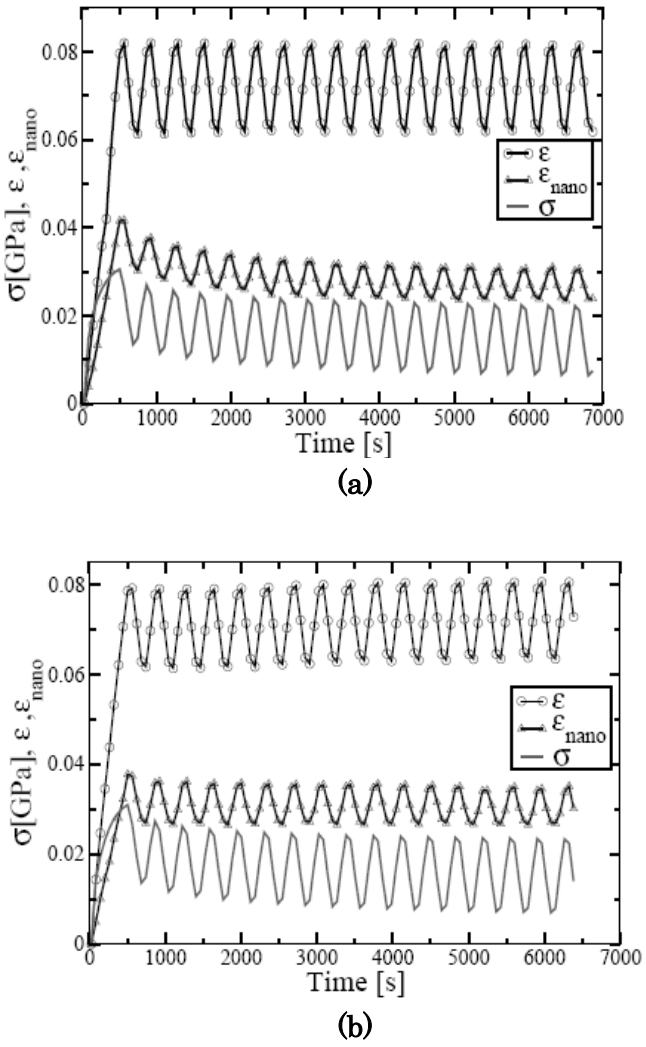

Figure 3: variation of macro and nano parameters during load cycling, a) Moplen & b) Mopnan

For both materials the elliptical peaks weaken in intensity considerably as the mechanical load is applied. As the Moplen is deformed, the drop-shape peaks move toward the center and turn into a meridional streak. In the case of the Mopnan sample the drop-shape two-point pattern exhibits clear maxima even at the end of the experiment. Thus, for the pure PP the application of mechanical strain causes considerable spreading of the long-period distribution (peak into streak), whereas the blending with CNT appears to considerably decrease this dispersion of long periods (peak remains peak).

In order to obtain more information about the microstructural variations, the nanoscopic strain ε_{nano}, is calculated based on the variation of the number-average long period, as determined from the CDFs. Strain, nanoscopic strain, and stress during load cycling are presented in Figs. 3a and 3b for Moplen and Mopnan samples, respectively. Both samples show little macroscopic fatigue which is inferred from the mild decrease in the stress level from cycle to cycle. The

nanoscopic strain is smaller than the macroscopic strain in both cases. The nanoscopic fatigue is readily assessed from the decrement of successive maxima in $\varepsilon_{nano}(t)$. Obviously, the blending with CNT effectively decreases the nanoscopic fatigue of the material.

In order to explain this finding we speculate that the stress is effectively transferred from the polypropylene matrix to the nanotubes, and a reinforced semi-crystalline layer system experiences a lower stress in comparison with the semi-crystalline system of the pure polypropylene. Hence, the carbon nanotubes stabilize the nano-structure of polypropylene and improve fatigue properties of this material.

Microfibrillar reinforced composites: SAXS patterns and corresponding CDFs of the MFC sample at different steps of deformation are shown in Fig. 4. In order to have more information about the variation of nano-structure, the nanoscopic strain ε_{nano}, is extracted from peak positions on the meridian. Stress, strain, nanoscopic strain, and scattering power of the chosen sample cycled about low pre-strain (2%) and high pre-strain (6%) are shown in Figs. 5 and 6, respectively. In the case of low pre-strain the material shows weak fatigue only, whereas the same material subjected to a higher pre-strain shows very strong fatigue which can be easily inferred from the decrease of the stress σ, from cycle to cycle. In Fig. 4, the macroscopic strain ε, becomes negative after ca. 40 min. This observation may be explained by viscous flow of the material. During the further course of the experiment (t > 80 min) this fatigue flow even causes the sample to become slack. It bends in each cycle close to the lower dead centers. As a result, the apparent ε drops considerably.

No significant phase shift is observed between ε_{nano}, σ, and ε both for low pre-strain and for high pre-strain. Thus, these quantities predominantly reflect the forced oscillation of the cross-heads. On the other hand, for both pre-strains at small deformations, ε_{nano} and ε are comparable, but at higher deformations ε_{nano} is remarkably smaller than ε.

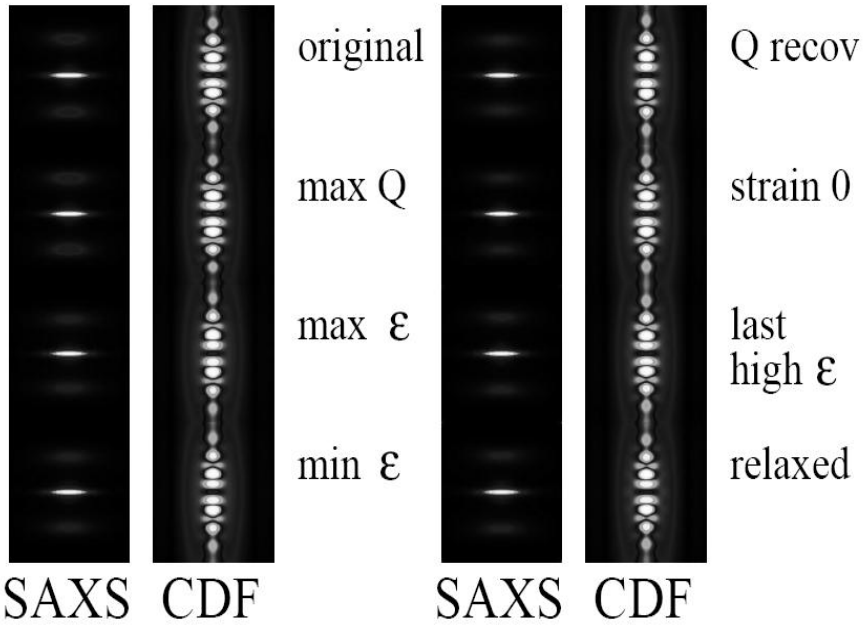

Figure 4. Selected SAXS patterns $I(s_{12}, s_3)$ and CDFs $|z(r_{12}, r_3)|$ from the experiment in which the load cycling has been performed on high pre-strain ("high-cycling experiment"). Intensities are on logarithmic scale. Displayed regions: $-0.1\text{nm}^{-1} < s_{12}, s_3 < 0.1\text{nm}^{-1}$, $-75\text{ nm} < r_{12}, r_3 < 75\text{ nm}$

Compared to other parameters the evolution of the scattering power, Q, appears to be different. At the beginning of both experiments the scattering power is increasing. Eq. (2) shows that it is impossible to assign the reason for the increase of the integral quantity Q to one of the structural parameters in the equation, unless one takes advantage of the anisotropy of the scattering patterns. Based on the integral quantity alone, it would not even be possible to decide if an increase or a decrease of crystallinity or contrast are the reason for a specific change of Q.

Nevertheless, even from a first visit to the data some heuristic assessments can be made. When in the low-cycling experiment (Fig. 5) the first top dead-center is reached (t = 4min), $Q(t)$ has just passed a maximum. In the high-cycling experiment (Fig. 6) the first top dead-center is much later – at higher strain ε and at higher stress σ. At this time, $Q(t)$ has already dropped considerably below the initial scattering power. In the following cycles an almost negligible Q-oscillation is considerably amplified by the external load, until its amplitude appears saturated from the 10th cycle. This is completely different in the low-cycling experiment (Fig. 5), where the amplitude of the Q-oscillation is high and constant from the first cycle to the last. Comparison of these observations indicates that the initial increase of Q is related to a fortification of the nanostructure, similar to the strain-induced crystallization that has been detected in an earlier study of hard-elastic

polypropylene [10], whereas the subsequent drop of Q appears to be indicative for structural deterioration. In a recent study [4] on continuous straining of the microfibrillar reinforced HDPE/PA-blends we have already carried out a detailed analysis of the anisotropic scattering patterns and have reported that the initial nanostructure of the polyethylene in the HDPE/PA-blends is rather heterogeneous. There fortification at low strain is accomplished by a mechanism, in which the crystalline domains become wedged. At higher strain this wedged structure is broken, crystallites are destroyed, and the lateral correlation among the domains is lost. Now in the high pre-strain load-cycling experiment the evolution of $Q(t)$ indicates some structural adaption process. The last part of the initial increasing load ramp appears to deteriorate the original nanostructure. Then the cycling appears to "teach" the material an adapted nanostructure that, again, responds "elastically" on the forced external load cycles.

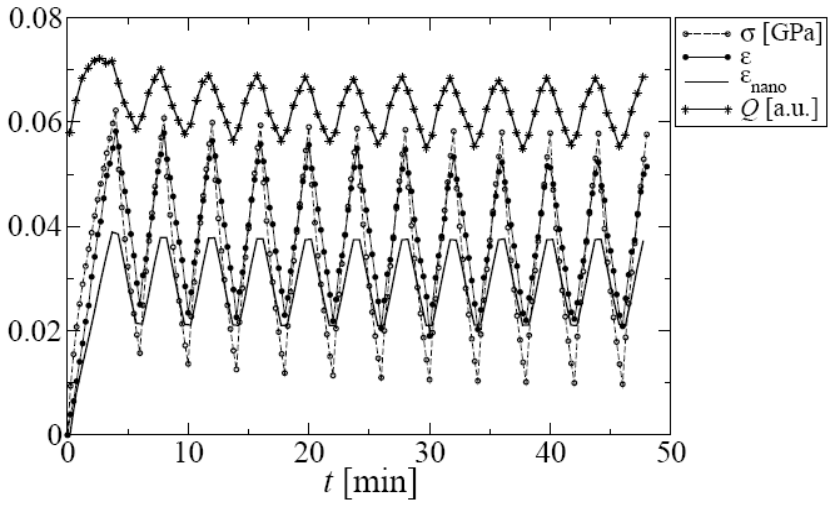

Figure 5. Macro/nanoscopic parameters of HDPE/PA6 (80/20) cycled about low pre-strain

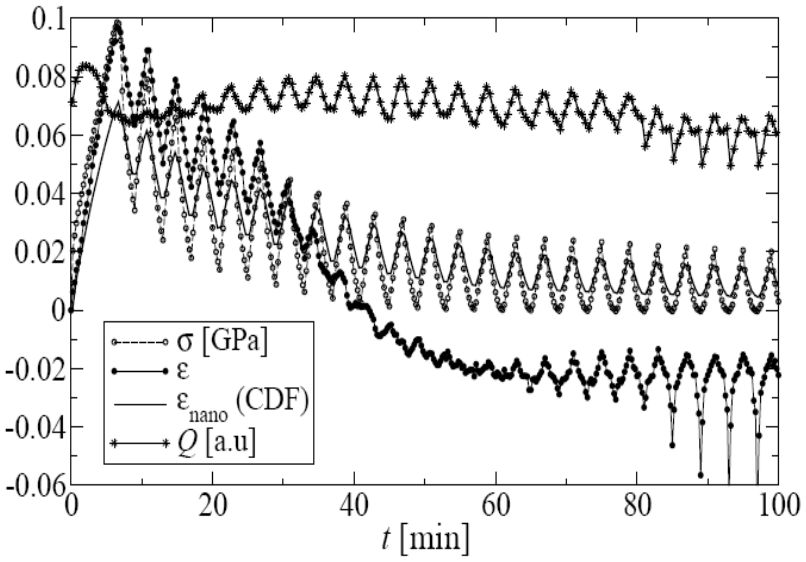

Figure 6. Macro/nanoscopic parameters of HDPE/PA6 (80/20) cycled about high pre-strain

Thermoplastic polyurethane elastomers: SAXS patterns and corresponding CDFs of different TPU samples are presented in Figs. 7-9. All samples are oriented in their initial state. This orientation is caused during injection molding process. However, the meridional peaks are weaker and broader for undeformed TPU235 in comparison with the samples molded at lower temperature. The lower intensity of the peaks is due to less developed phase separation and is in line with the mechanical data. The lower orientation of TPU235 can also be due to lower melt viscosity at higher temperature. As the samples are deformed, the meridional peaks become weaker and also an equatorial streak develops. The decrease of peak intensity indicates deterioration of hard segment domains. The development of the equatorial streak can be due to fibrillation of soft segment phase or growth of microvoids and crazes.

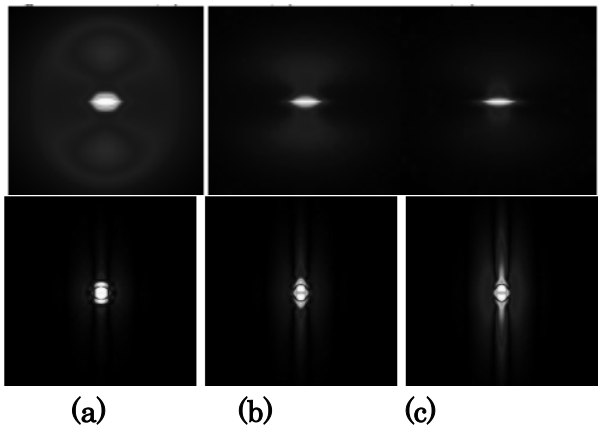

Figure 7. SAXS patterns (1st row) and corresponding CDFs (2nd row) of TPU205 sample: (a) initial state, (b) half maximum strain (c) maximum strain

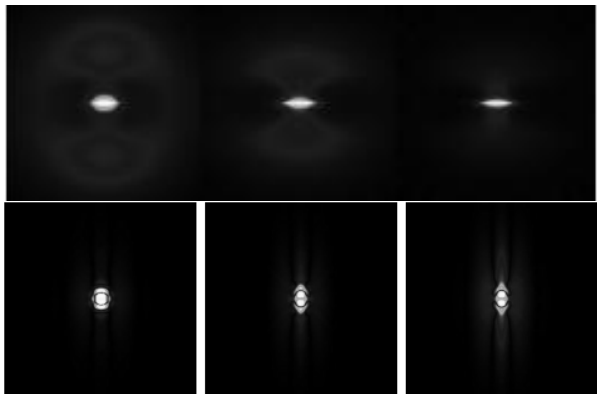

Figure 8. SAXS patterns (1st row) and corresponding CDFs (2nd row) of TPU215 sample: (a) initial state, (b) half maximum strain (c) maximum strain

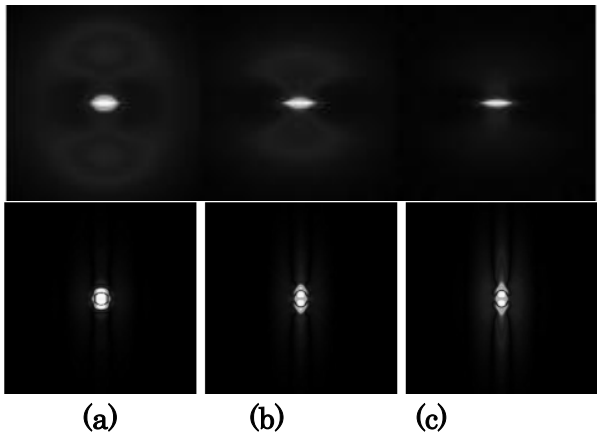

Figure 9. SAXS patterns (1st row) and corresponding CDFs (2nd row) of TPU235 sample: (a) initial state, (b) half maximum strain (c) maximum strain

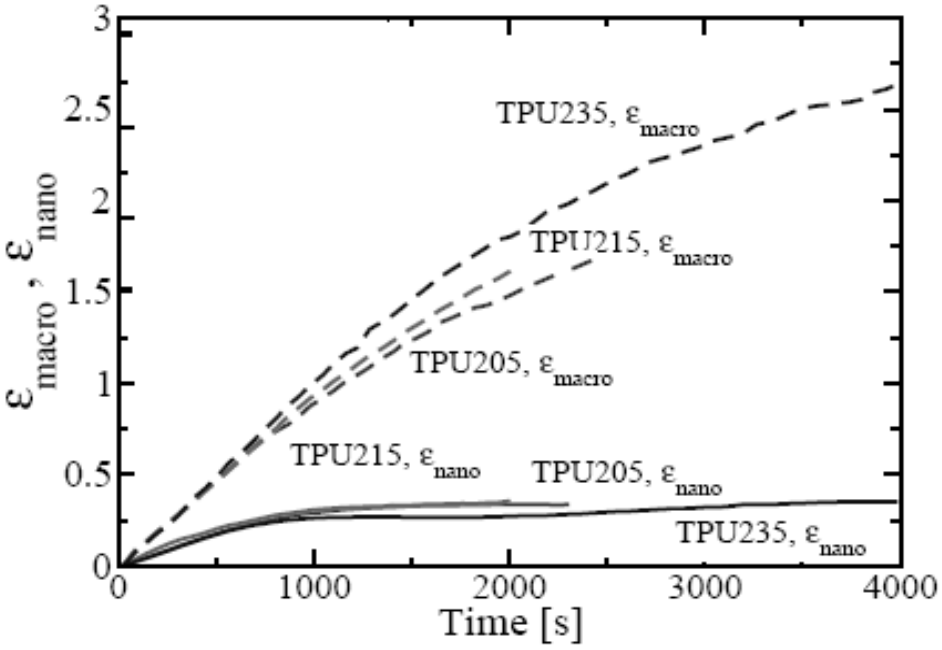

Figure 10. Macroscopic and nanoscopic strain of different TPU samples

In order to obtain more information about the nanoscopic variations, long periods of structural moieties are extracted from peak positions in CDFs. It is seen that the nanoscopic strain is quite smaller than the macroscopic strain, Fig. 10.

Discussion:

We have observed that the nanoscopic strain is smaller than macroscopic strain for all the studied samples. To explain this observation we propose the following mechanism which is depicted in Fig. 11. In a semicrystalline polymer two different amorphous regions can be distinguished; i) a sandwiched amorphous phase which consists of amorphous chain segments between lamellae and ii) free amorphous regions which are far away from crystallites. When a semicrystalline polymer is stressed, crystallites resist deformation due to their higher modulus in comparison with the surrounding amorphous phase, thus, the deformation mainly takes place in the amorphous regions. At small macroscopic strains the sandwiched and the free amorphous regions are deformed almost to the same extent, while at higher deformations the sandwiched domains resist further deformation due to the effect of tie molecules which are stretched to the highest possible extent. Thus, the deformation predominantly occurs in the free amorphous region. Keeping in mind that ε_{nano} is determined from the long period between lamellae, it increases to the same extent of ε at small deformations (affine deformation), while its variation rate

slows down at large deformations (non-affine deformation).

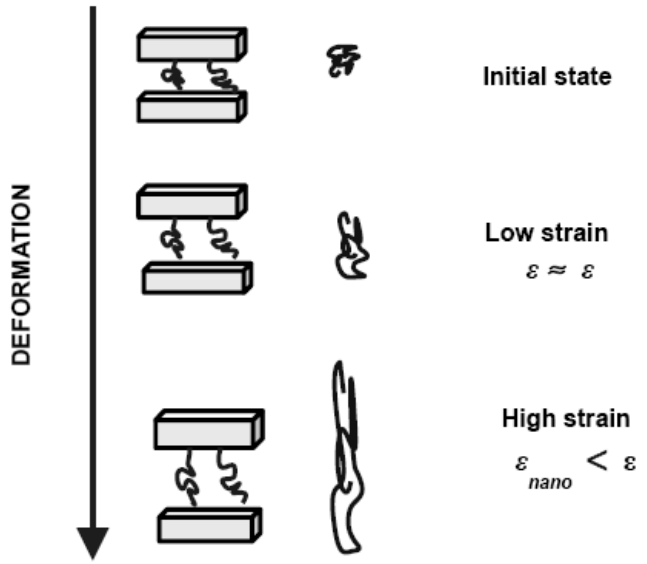

Figure 11. Schematic presentation of deformation mechanism in a semicrystalline polymer

Conclusions

Four different types of samples have been tested to cover a wide range of polymeric materials and to draw some conclusions about the behavior and transient structures of semi-crystalline polymers under tensile load. The macroscopic strain is obtained from the video frames and simultaneously the variations of microstructure is recorded by SAXS patterns. The CDF is computed and from the variations of long period peak on the CDFs the nanoscopic strain is estimated. For all of the studied materials the nanoscopic strain is smaller than the macroscopic strain, except for very small deformations. This is attributed to the resistance of taut tie molecules against deformation and heterogeneous deformation of the material at the nano-scale. Further studies on other types of materials and other mechanical properties (eg. Creep resistance) are in progress.

Acknowledgments

The authors thank the Hamburg Synchrotron Radiation Laboratory (HASYLAB) for beam time granted in the frame of project II-04-039. This work has been supported by the 7th framework program of the European Union (Project NANOTOUGH FP7-NMP-2007-LARGE). We gratefully acknowledge the preparation of the materials by JC Christiansen et al. at Aalborg University (Denmark), Z. Denchev et al. University of Minho (Portugal) and A. Frick et al. Hochschule Aalen (Germany).

References

1. Denchev, Z.; Dencheva, N.; Funari, S.S.; Motovilin, M.; Schubert, T.; Stribeck, N., J. Polym. Sci. Part B: Polym. Phys., 48 (2010) 237-250
2. Zeinolebadi, A.; Stribeck, N., J. Phys. Conf. Ser., submitted
3. Stribeck, N.; Nöchel, U.; Funari, S.S.; Schubert, T.; Timmann, A., Macromol. Chem. Phys., 209 (2008) 1992–2002
4. Denchev Z Z and Dencheva N V 2008 *Polym. Inter.* **57** 11–22
5. Stribeck N 2007 *X-Ray Scattering of Soft Matter* (Heidelberg, New York: Springer)
6. Toki S, Sics I, Burger C, Fang D, Liu L, Hsiao B S, Datta S and Tsou A H 2006 *Macromolecules* **39** 3588–3597
7. Brown H R, Kramer E J and Bubeck R A 1988 *J. Mater. Sci.* **23** 248–252
8. Heeley, E.L.; Morgovan, A.C.; Bras, W.; Dolbnya, I.P.; Gleeson, A.J.; Ryan, A.J., , Phys. Chem. Comm., 5 (2002) 158-160
9. Gerasimov, V.I.; Genin, Y.V.; Kitaigorodsky, A.I.; Tsvankin, D.Y., , Kolloid-Z. u. Z. Polymere, 250 (1972) 518-529
10. Stribeck N and Nöchel U 2008 *J. Appl. Cryst.* **41** 715–722